

Conformal mapping of some non-harmonic functions in transport theory

By Martin Z. Bazant

Department of Mathematics

Massachusetts Institute of Technology, Cambridge, MA 02139 USA

and

Laboratoire de Physico-chimie Théorique

École Supérieure de Physique et de Chimie Industrielles

10 rue Vauquelin, 75231 Paris, France.

Conformal mapping has been applied mostly to harmonic functions, i.e. solutions of Laplace's equation. In this paper, it is noted that some other equations are also conformally invariant and thus equally well suited for conformal mapping in two dimensions. In physics, these include steady states of various nonlinear diffusion equations, the advection-diffusion equations for potential flows, and the Nernst-Planck equations for bulk electrochemical transport. Exact solutions for complicated geometries are obtained by conformal mapping to simple geometries in the usual way. Novel examples include nonlinear advection-diffusion layers around absorbing objects and concentration polarizations in electrochemical cells. Although some of these results could be obtained by other methods, such as Boussinesq's stream line coordinates, the present approach is based on a simple unifying principle of more general applicability. It reveals a basic geometrical equivalence of similarity solutions for a broad class of transport processes and paves the way for new applications of conformal mapping, e.g. to non-Laplacian fractal growth.

Keywords: conformal mapping, non-harmonic functions, nonlinear diffusion, advection-diffusion, electrochemical transport

1. Introduction

Complex analysis is one of the most beautiful subjects in mathematics, and, in spite of involving imaginary numbers, it has remarkable relevance for 'real' applications. One of its most useful techniques is conformal mapping, which transforms planar domains according to analytic functions, $w = f(z)$, with $f'(z) \neq 0$. Geometrically, such mappings induce upon the plane a uniform, local stretching by $|f'(z)|$ and a rotation by $\arg f'(z)$. This 'amplitwist' interpretation of the derivative implies conformality, the preservation of angles between intersecting curves (Needham 1997).

The classical application of conformal mapping is to solve Laplace's equation,

$$\nabla^2 \phi = 0; \quad (1.1)$$

ie. to determine harmonic functions, in complicated planar domains by mapping to simple domains. The method relies on the conformal invariance of Eq. (1.1), which remains the same after a conformal change of variables. Before the advent of computers, important analytical solutions were thus obtained for electric fields in capacitors, thermal fluxes around pipes, inviscid flows past airfoils, etc. (Needham 1997; Churchill & Brown 1990; Batchelor 1967). Today, conformal mapping is still used extensively in numerical methods (Trefethen 1986).

Currently in physics, a veritable renaissance in conformal mapping is centering around ‘Laplacian-growth’ phenomena, in which the motion of a free boundary is determined by the normal derivative of a harmonic function. Continuous problems of this type include viscous fingering, where the pressure is harmonic (Saman & Taylor 1958; Bensimon et al. 1986; Saman 1986), and solidification from a supercooled melt, where the temperature is harmonic in some approximations (Kessler et al. 1988; Cummings et al. 1999). Such problems can be elegantly formulated in terms of time-dependent conformal maps, which generate the moving boundary from its initial position. This idea was first developed by Polubarinova-Kochina (1945a; 1945b) and Galin (1945) with recent interest stimulated by Shraiman & Bensimon (1984) focusing on finite-time singularities and pattern selection (Howison 1986; Tanveer 1987; Dai et al. 1991; Ben Amar 1991; Howison 1992; Tanveer 1993; Ben Amar & Brenner 1996; Ben Amar & Poire 1999; Feigenbaum et al. 2001).

Stochastic problems of a similar type include diffusion-limited aggregation (DLA) (Witten & Sander 1981) and dielectric breakdown (Niemeyer et al. 1984). Recently, Hastings & Levitov (1998) proposed an analogous method to describe DLA using iterated conformal maps, which initiated a flurry of activity applying conformal mapping to Laplacian fractal-growth phenomena (Davidovitch et al. 1999, 2000; Barra et al. 2002a, 2002b; Stepanov & Levitov 2001; Hastings 2001; Somfai et al. 1999; Ball & Somfai 2002). One of our motivations here is to extend such powerful analytical methods to fractal growth phenomena limited by non-Laplacian transport processes.

Compared to the vast literature on conformal mapping for Laplace’s equation, the technique has scarcely been applied to any other equations. The difficulty with non-harmonic functions is illustrated by Helmholtz’s equation,

$$\nabla^2 \psi = f; \quad (1.2)$$

which arises in transient diffusion and electromagnetic radiation (Morse & Feshbach 1953). After conformal mapping, $w = f(z)$, it acquires a cumbersome, non-constant coefficient (the Jacobian of the map),

$$\nabla^2 \psi \nabla^2 \bar{z} = f; \quad (1.3)$$

Similarly, the bi-harmonic equation,

$$\nabla^2 \nabla^2 \psi = 0; \quad (1.4)$$

which arises in two-dimensional viscous flows (Batchelor 1967) and elasticity (Muskhelishvili 1953), transform with an extra Laplacian term (see below),

$$\nabla^4 \psi \nabla^2 \bar{z} = 4 \nabla^2 \nabla^2 \psi \nabla^2 \bar{z}; \quad (1.5)$$

In this special case, conformal mapping is commonly used (e.g. Chan et al. 1997; Crowdy 1999, 2002; Barra et al. 2002b) because solutions can be expressed in terms of analytic functions in Goursat form (Muskhelishvili 1953). Nevertheless, given the singular ease of applying conformal mapping to Laplace's equation, it is natural to ask whether any other equations share its conformal invariance, which is widely believed to be unique.

In this paper, we show that certain systems of nonlinear equations, with non-harmonic solutions, are also conformally invariant. In section 2, we give a simple proof of this fact and some of its consequences. In section 3, we discuss applications to nonlinear diffusion phenomena and show that single conformally invariant equations can always be reduced to Laplace's equation (which is not true for coupled systems). In section 4, we apply conformal mapping to nonlinear advection-diffusion in a potential flow, which is equivalent to stream line coordinates in a special case (Boussinesq 1905). In section 5, we apply conformal mapping to nonlinear electrochemical transport, apparently for the first time. In section 6, we summarize the main results. Applications to non-Laplacian fractal growth are a common theme throughout the paper. (See sections 2, 4, and 6.)

2. Mathematical Theory

(a) Conformal mapping without Laplace's Equation?

The standard application of conformal mapping is based on two facts:

1. Any harmonic function, u , in a singly connected planar domain, D_w , is the real part of an analytic function, f , the 'complex potential' (which is unique up to an additive constant): $u = \text{Re}(f(w))$.
2. Since analyticity is preserved under composition, harmonicity is preserved under conformal mapping, so $u \circ f = \text{Re}(f(z))$ is harmonic in $D_z = f^{-1}(D_w)$.

Presented like this, it seems that conformal mapping is closely tied to harmonic functions, but Fact 2 simply expresses the conformal invariance of Laplace's equation: A solution, $u(w)$, is the same in any mapped coordinate system, $u(f(z))$. Fact 1, a special relation between harmonic functions and analytic functions, is not really needed. If another equation were also conformally invariant, then its non-harmonic solutions, $u(w; \bar{w})$, would be preserved under conformal mapping in the same way, $u(f(z); \bar{f}(z))$. (See Fig. 1.)

In order to seek such non-Laplacian invariant equations, we review the transformation properties of some basic differential operators. Following Argyand and Gauss, it is convenient to represent two-dimensional vectors, $a = a_x \hat{x} + a_y \hat{y}$, as complex numbers, $a = a_x + a_y i$. We thus express the gradient vector operator in the plane as a complex scalar operator,

$$\mathbf{r} = \hat{x} \frac{\partial}{\partial x} + \hat{y} \frac{\partial}{\partial y} \quad ! \quad r = \frac{\partial}{\partial x} + i \frac{\partial}{\partial y}; \quad (2.1)$$

which has the essential property that $\mathbf{r}f = 0$ if and only if f is analytic, in which case, $\mathbf{r}f = 2f^0$ (Needham 1997). Since $a \cdot b = \text{Re} \bar{a}b$, the Laplacian operator can

be written $\nabla^2 = \frac{\partial^2}{\partial x^2} + \frac{\partial^2}{\partial y^2} = \frac{1}{2} \mathbf{r} \cdot \bar{\mathbf{r}}$ is more common in the mathematical literature, we prefer \mathbf{r} for applications in transport theory because gradients play a central role.

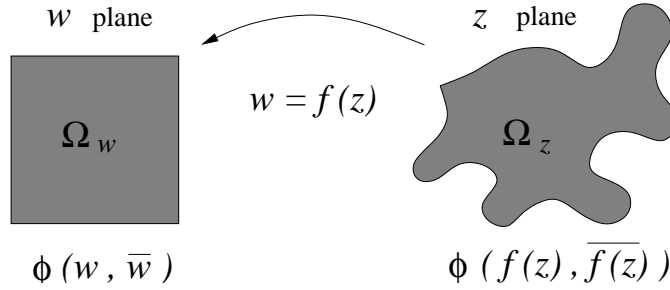


Figure 1. Conformal mapping, $w = f(z)$, of a solution, ϕ , to a conformally invariant equation from a complicated domain, Ω_z , and a simple domain, Ω_w .

be expressed as, $r_z \bar{r}_z = \text{Re} \bar{r} r = \bar{r} r$ (if mixed partial derivatives can be taken in any order). Similarly, the advection operator, which acts on two real functions r and c , takes the form, $r_z c = \text{Re} (r_z) \bar{r}_z c$.

Under a conformal mapping of the plane, $w = f(z)$, the gradient transforms as, $r_z = \bar{f}^0 r_w$. This basic fact, combining the amplification property and the chain rule, makes it easy to transform differential operators (Needham 1997). The Laplacian transforms as,

$$r_z \bar{r}_z = (r_z f^0) \bar{r}_w + \bar{f}^0 \bar{f}^0 r_w \bar{r}_w = \bar{f}^0 \bar{f}^0 r_w \bar{r}_w \quad (2.2)$$

where $r_z f^0 = 0$ because f^0 is also analytic. This immediately implies the conformal invariance of Laplace's equation (1.1), and the non-invariance of Helmholtz's equation (1.2). The transformation of the bi-harmonic equation (1.4) in Eq. (1.5) is also easily derived with the help of Needham's identity, $\bar{f}^0 f^0 = 4 \bar{f}^0 \bar{f}^0$, applied to f^0 .

Everything in this paper follows from the simple observation that the advection operator transforms just like the Laplacian,

$$\text{Re} (r_z) \bar{r}_z c = \bar{f}^0 \bar{f}^0 \text{Re} (r_w) \bar{r}_w c \quad (2.3)$$

Each operator involves a dot product of two gradients, so the same Jacobian factor, $\bar{f}^0 \bar{f}^0$, appears in both cases. The transformation laws, Eq. (2.2) and Eq. (2.3), are surely well known, but it seems that some general implications have been overlooked, or at least not fully exploited in physical applications.

(b) Conformally Invariant Systems of Equations

The identities (2.2) and (2.3) imply the conformal invariance of any system of equations of the general form,

$$\sum_{i=1}^N a_i(\mathbf{r}) r_i^2 + \sum_{j=1}^N a_{ij}(\mathbf{r}) r_i r_j A = 0 \quad (2.4)$$

where the coefficients $a_i(\mathbf{r})$ and $a_{ij}(\mathbf{r})$ may be nonlinear functions of the unknowns, $\mathbf{r} = (r_1; r_2; \dots; r_N)$, but not of the independent variables or any derivatives of the unknowns. Thus we arrive at our main result:

Theorem 2.1. (Conformal Mapping Theorem.) Let $(w; \bar{w})$ satisfy Eq. (2.4) in a domain w of the complex plane, and let $w = f(z)$ be a conformal mapping from z to w . Then $(f(z); \bar{f}(z))$ satisfies Eq. (2.4) in z .

Whenever the system (2.4) can be solved analytically in some simple domain, the Theorem produces a family of exact solutions for all topologically equivalent domains. Otherwise, it allows a convenient numerical solution to be mapped to more complicated domains of interest. This is an enormous simplification for free boundary problems, where the solution in an evolving domain can be obtained by time-dependent conformal mapping to a single, static domain.

Conformal mapping is most useful when the boundary conditions are also invariant. Dirichlet ($\phi = \text{constant}$) or Neumann ($\hat{n} \cdot \mathbf{r} = 0$) conditions are typically assumed, but here we consider the straight-forward generalizations,

$$b_i(\mathbf{r}) = 0 \quad \text{and} \quad \sum_{j=1}^N b_{ij}(\mathbf{r}) (\hat{n} \cdot \mathbf{r}_j)^i = 0 \quad (2.5)$$

respectively, where $b_i(\mathbf{r})$ and $b_{ij}(\mathbf{r})$ are nonlinear functions of the unknowns, ϕ_i is a constant, and \hat{n} is the unit normal. The conformal invariance of the former is obvious, so we briefly consider the latter.

It is convenient to locally transform a vector field, \mathbf{F} , along a given contour as, $\tilde{\mathbf{F}} = t\bar{\mathbf{F}}$, so that $\text{Re } \tilde{\mathbf{F}}$ and $\text{Im } \tilde{\mathbf{F}}$ are the projections onto the unit tangent, $\mathbf{t} = d\mathbf{z}/|dz|$, and the (right-handed) unit normal, $\mathbf{n} = -it$, respectively. Since the tangent transforms as, $t_w = t_z f^0 = \tilde{f}^0 \mathbf{j}$, and the gradient as, $\mathbf{r}_z = \bar{f}^0 \mathbf{r}_w$, we find, $\tilde{\mathbf{r}}_z = \tilde{f}^0 \tilde{\mathbf{r}}_w$. The invariance of Eq. (2.5) follows after taking the imaginary part on the boundary contour.

(c) Gradient-Driven Flux Densities

Generalizing \mathbf{r} for Laplacian problems, we define a 'flux density' for solutions of Eq. (2.4) to be any quasi-linear combination of gradients,

$$\mathbf{F}_i = \sum_{j=1}^N c_{ij}(\mathbf{r}) \mathbf{r}_j; \quad (2.6)$$

where $c_{ij}(\mathbf{r})$ are nonlinear functions. The transformation rules above for the gradient apply more generally to any flux density,

$$\mathbf{F}_z = \bar{f}^0 \mathbf{F}_w \quad \text{and} \quad \tilde{\mathbf{F}}_z = \tilde{f}^0 \tilde{\mathbf{F}}_w; \quad (2.7)$$

These basic identities imply a curious geometrical equivalence between solutions to different conformally invariant systems:

Theorem 2.2. (Equivalence Theorem.) Let (1) and (2) satisfy equations of the form (2.4) with corresponding flux densities, $\mathbf{F}^{(1)}$ and $\mathbf{F}^{(2)}$, of the form (2.6). If $\mathbf{F}_z^{(1)} = a \mathbf{F}_z^{(2)}$ on a contour C_z for some complex constant a , then $\mathbf{F}_w^{(1)} = a \mathbf{F}_w^{(2)}$ on the image, $C_w = f(C_z)$, after a conformal mapping, $w = f(z)$.

An important corollary pertains to 'similarity solutions' of Eqs. (2.4) and (2.5) in which certain variables $f_i g$ involved in a flux density depend on only one Cartesian

coordinate, say w , after conformal mapping: $w = G(z)$. (Our examples below are mostly of this type.) Such special solutions share the same flux lines (level curves of $\text{Im } f(z)$) and iso-potentials (level curves of $\text{Re } f(z)$) in any geometry attainable by conformal mapping. They also share the same spatial distribution of flux density on an iso-potential, although the magnitudes generally differ.

An important physical quantity is the total normal flux through a contour, often called the Nusselt number, Nu . For any contour, C , we define a complex total flux, $I(C) = \int_C F^* dz = \int_C \bar{F} dz$, such that $\text{Re } I(C)$ is the integrated tangential flux and $\text{Im } I(C) = Nu(C)$. From Eq. (2.7) and $dw = f^0 dz$, we conclude, $I(C_z) = I(C_w)$. Therefore, flux integrals can be calculated in any convenient geometry.

This basic fact has many applications. For example, if F_w is constant on a contour $C_w = f(C_z)$, then for any conformal mapping, we have, $I(C_z) = I(C_w) = \ell(C_w) F_w$, where $\ell(C_w)$ is simply the length of C_w . For fluxes driven by gradients of harmonic functions, this is the basis for the method of iterated conformal maps for DLA, in which the 'harmonic measure' for random growth events on a fractal cluster is replaced by a uniform probability measure on the unit circle (Hastings & Levitov 1998).

More generally, a non-harmonic probability measure for fractal growth can be constructed for any flux law of the form (2.6) for fields satisfying Eq. (2.4). According to the results above, the growth probability is simply proportional to the normal flux density on the unit circle for the same transport problem after conformal mapping to the exterior of the unit disk. A nontrivial example is given below in section 4(c). This allows the Hastings-Levitov method to be extended to a broad class of non-Laplacian fractal-growth processes (Bazant, Choi & Davidovitch 2003).

(d) Conformal Mapping to Curved Surfaces

The Conformal Mapping Theorem is even more general than it might appear from our proof: The domain, z , may be contained in any two-dimensional manifold. This becomes clear from the recent work of Entov and Etingof (1991; 1997), who solved viscous fingering problems on various curved surfaces by conformal mapping to the complex plane, e.g. via stereographic projection from the Riemann sphere. They exploited the fact that Laplace's equation is invariant under any conformal mapping, $w = f(z)$, from the plane to a curved surface because the Laplacian transforms as $r_z^2 = J r_w^2$, where $J(f(z))$ is the Jacobian. The system (2.4) shares this general conformal invariance because the advection operator transforms in the same way, $r_z \cdot \nabla_z = J r_w \cdot \nabla_w$. The application of these ideas to non-Laplacian transport-limited growth phenomena on curved surfaces is work in progress with J. Choi and D. Crowdy; here we focus on conformal mappings in the plane, described by analytic functions.

3. Physical Applications to Diffusion Phenomena

Conformally invariant boundary-value problems of the form (2.4) and (2.5) commonly arise in physics from steady conservation laws,

$$\frac{\partial C_i}{\partial t} = r \quad F = 0; \quad (3.1)$$

for gradient-driven flux densities, Eq. (2.6), with algebraic ($\phi(c_i) = 0$) or zero-flux ($\nabla \cdot \mathbf{F} = 0$) boundary conditions, where c_i is the concentration and \mathbf{F}_i the flux of substance i . Hereafter, we focus on flux densities of the form,

$$\mathbf{F}_i = c_i \mathbf{u}_i - D_i(c_i) \nabla c_i; \quad \mathbf{u}_i \cdot \nabla = 0 \quad (3.2)$$

where $D_i(c_i)$ is a nonlinear diffusivity, \mathbf{u}_i is an irrotational vector field causing advection, and ϕ is a (possibly non-harmonic) potential. Examples include advection-diffusion in potential flows and bulk electrochemical transport.

Before discussing these cases of coupled dependent variables, it is instructive to consider nonlinear diffusion in only one variable. The most general equation of the type (2.4) for one variable is,

$$a(c) r^2 c = \nabla \cdot \mathbf{f}; \quad (3.3)$$

This equation arises in the Stefan problem of dendritic solidification, where c is the dimensionless temperature of a supercooled melt and $a(c)$ is Ivantsov's function, which implicitly determines the position of the liquid-solid interface via $a(c) = 1$ (Ivantsov 1947). In two dimensions, Bedia & Ben Amar (1994) prove the conformal invariance of Eq. (3.3) and then study similarity solutions, $c(\zeta) = G(\zeta)$, by conformal mapping, $w = \zeta + i\eta$, to a plane of parallel flux lines,

$$a(G) G'' = (G')^2; \quad (3.4)$$

where an ordinary differential equation is solved.

More generally, reversing these steps, it is straight-forward to show that any monotonic solution of Eq. (3.4) produces a nonlinear transformation, $c = G(\zeta)$, from Eq. (3.3) to Laplace's equation (1.1), which implies conformal invariance. There are several famous examples. For steady concentration-dependent diffusion,

$$\nabla \cdot (\mathbf{D}(c) \nabla c) = 0; \quad (3.5)$$

it is Kirchhoff's transformation (Crank 1975), $\zeta = G^{-1}(c) = \int_0^c D(x) dx$. For Burgers' equation in an irrotational flow ($\mathbf{u} = \nabla \phi$),

$$\frac{\partial u}{\partial t} + \mathbf{u} \cdot \nabla u = \nabla^2 u; \quad (3.6)$$

which is equivalent to the KPZ equation without noise (Kardar et al. 1986),

$$\frac{\partial h}{\partial t} = \nabla^2 h + \frac{1}{2} \nabla \cdot \mathbf{h}^2; \quad (3.7)$$

it is the Cole-Hopf transformation (Whitham 1974), $\zeta = G^{-1}(h) = e^{h/2}$, which yields the diffusion equation, $\frac{\partial \phi}{\partial t} = \nabla^2 \phi$, and thus Laplace's equation in steady state.

In summary, the general solutions to Equation (3.3) are simply nonlinear functions of harmonic functions, so, in the case of one variable, our theorems can be easily understood in terms of standard conformal mapping. For two or more coupled variables, however, this is no longer true, except for special similarity solutions. The following sections discuss some truly non-Laplacian physical problems.

4. Steady Advection-Diffusion in a Potential Flow

We begin with a well known system of the form (2.5), the only one to which conformal mapping has previously been applied (see below), albeit not in the present, more general context. Consider the steady diffusion of particles or heat passively advected in a potential flow, allowing for a concentration-dependent diffusivity. For a characteristic length, L , speed, U , concentration, C , and diffusivity, $D(C)$, the dimensionless equations are

$$\nabla^2 \psi = 0 \quad \text{and} \quad \text{Pe} \nabla \cdot \mathbf{r} c = \nabla \cdot (\mathbf{b}(c) \nabla c); \quad (4.1)$$

where ψ is the velocity potential (scaled to UL), c is the concentration (scaled to C), $\mathbf{b}(c)$ is the dimensionless diffusivity, and $\text{Pe} = UL/D$ is the Peclet number. The latter equation is a steady conservation law for the dimensionless flux density, $\mathbf{F} = \text{Pe} \nabla \cdot \mathbf{r} c - \mathbf{b}(c) \nabla c$ (scaled to $DC = L$). For $\mathbf{b}(c) = 1$, these classical equations have been studied recently in two dimensions, e.g. in the contexts of tracer dispersion in porous media (Koplik et al. 1994, 1995), vorticity diffusion in strained wakes (Eames & Bush 1999; Hunt & Eames 2002), thermal advection-diffusion (Morgan & Behan 1994; Sen & Yang 2000), and dendritic solidification in flowing melts (Kornev & Mukhamadullina 1994; Cummings et al. 1999).

(a) Similarity Solutions for Absorbing Leading Edges

Let us rederive a classical solution in the upper half plane, $w = \zeta + i\eta$ ($\eta > 0$), which we will then map to other geometries. As shown in the top left panel of Fig. 2, consider a straining velocity field, $\mathbf{u} = \text{Re} \, \zeta$, $\mathbf{u} = w^2$, $u = \overline{w}^0 = 2\overline{w} = 2\zeta - 2i\eta$, which advects a concentrated fluid, $c(\zeta; 1) = 1$, toward an absorbing wall on the real axis, $c(\zeta; 0) = 0$. Since the η -component of the velocity (toward the wall) is independent of ζ , as are the boundary conditions, the concentration depends only on η . The scaling function, $c(\zeta; \text{Pe}) = S(\text{Pe} \eta) = S(\sim)$, satisfies

$$2\sim S^0 = (\mathbf{b}(S) S^0)^0; \quad S(0) = 0; \quad S(1) = 1; \quad (4.2)$$

which is straightforward to solve, at least numerically. For $\mathbf{b}(S) = 1$, Equation (4.2) has a simple, analytical solution, $S(\sim) = \text{erf}(\sim)$ (e.g. Cummings et al. 1999).

If extended to the entire w -plane, where two fluids of different concentrations flow towards each other, this solution also describes a Burgers' vortex sheet under uniform strain (Burgers 1948). In that case, $(\zeta; \eta; c)$ is a three-dimensional velocity field satisfying the Navier-Stokes equations, and Pe is the Reynolds number. Inserting a boundary, such as the stationary wall on the real axis, however, is not consistent with Burgers' solution because the no-slip condition cannot be satisfied. The wall is crucial for conformal mapping to other geometries because it enables singularities to be placed in the lower half plane.

For every conformal map to the upper half plane, $w = f(z)$, we obtain a solution,

$$\psi = \text{Re} f(z)^2 \quad \text{and} \quad c = S \left(\frac{\text{Pe}}{2} \text{Im} f(z) \right) \quad \text{for} \quad \text{Im} f(z) \geq 0 \quad (4.3)$$

which describes the nonlinear advection-diffusion layer in a potential flow of concentrated fluid around the leading edge of an absorbing object. For a linear diffusivity, $S(\sim) = \text{erf} \sim$, various examples are shown in Fig. 2. The choice, $f(z) = \sqrt{z}$, a, in

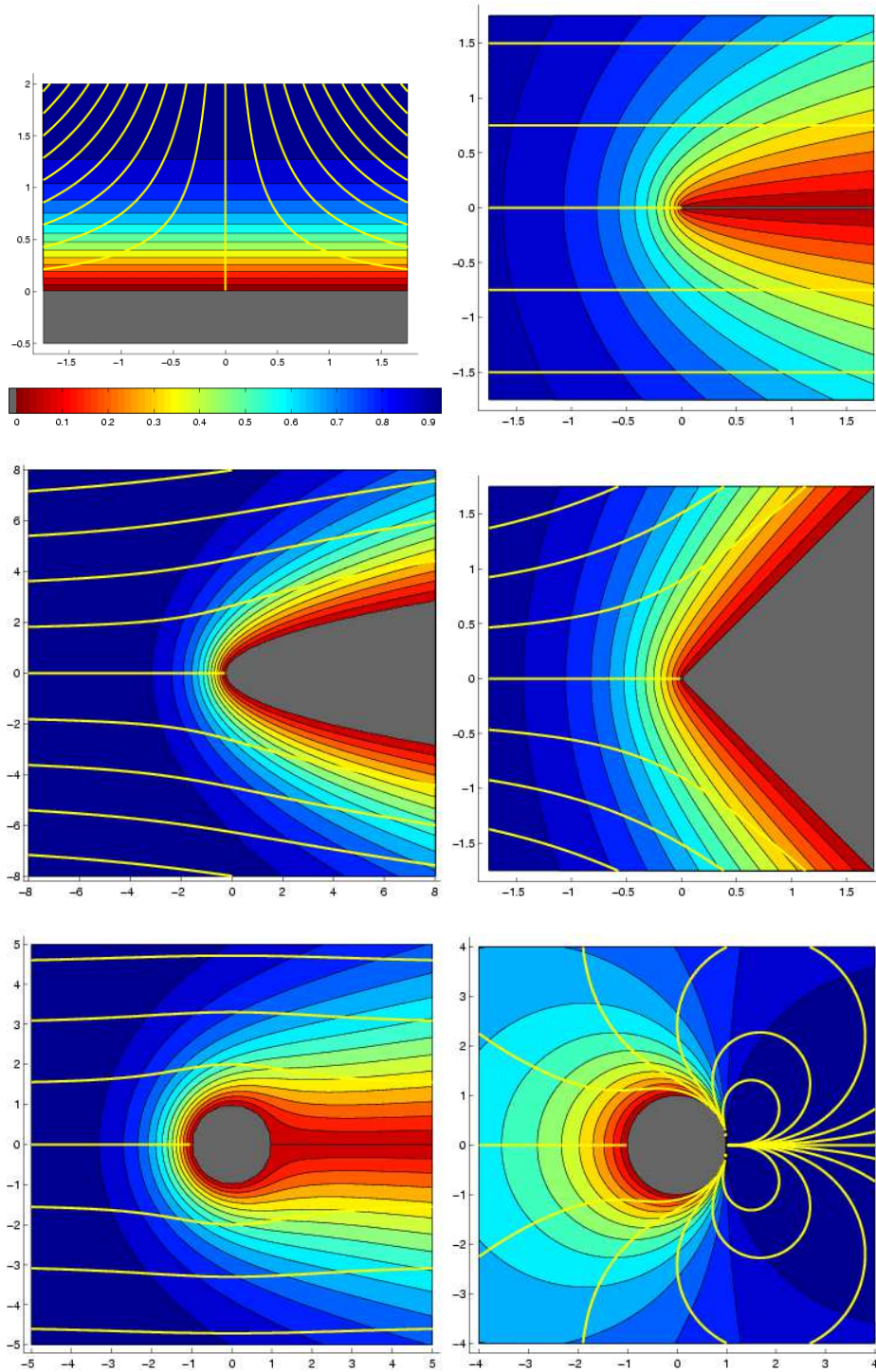


Figure 2. Concentration profiles (contour plots) and potential-flow streamlines (yellow) for steady, linear advection-diffusion layers around various absorbing surfaces (gray) at $Pe = 1$. All solutions are given by Eq. (4.3), where $w = f(z)$ is a conformal map to the upper halfplane (top left). The color scale applies to all panels in Figs. 2 and 3.

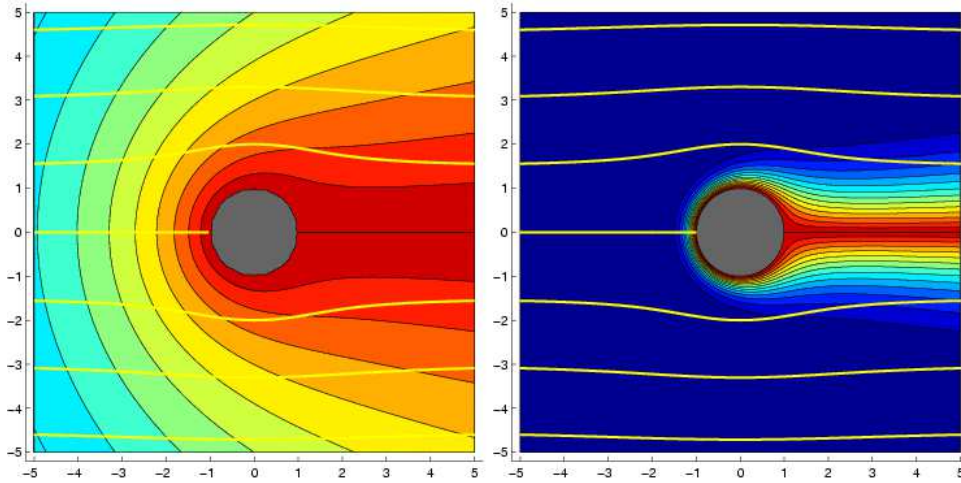


Figure 3. The steady linear advection-diffusion layer around a cylindrical rim on a flat plate at $Pe = 0.1$ (left) and $Pe = 10$ (right).

the middle left panel, describes a parabolic leading edge, $x = (y/2)^2$, where $y = \text{Im } z$. The limit of uniform flow past a half plate ($a = 0$), in the upper right panel is a special case discussed below.

Another classical map, $f(z) = z^{1/2}$, describes a wedge of opening angle π , as shown in the middle right panel for $\alpha = \pi/2$ (after a rotation by $\pi/4$). The half plate ($\alpha = 0$) and the flat wall ($\alpha = \pi$) discussed above are special cases. The diffusive flux on the surface from Eq. (4.8), $j_x = -D \partial \phi / \partial x$, is singular for acute angles, $\alpha < \pi/2$. The geometry-dependent exponent, $\beta = (1 - \alpha/\pi)/2$, is the same for pure diffusion to the wedge, $\phi = \text{Im } f(z)$ (Barenblatt 1995). This insensitivity to Pe is a signature of the Equivalence Theorem, as explained below.

The less familiar mapping, $f(z) = z^{1/2} + z^{-1/2}$, which plays a crucial role in non-Laplacian growth problems (see below), places a cylindrical rim on the end of a semi-infinite flat plate, as shown in the lower left panel. The solution has a pleasing form in polar coordinates,

$$\phi = r + \frac{1}{r} \cos \theta \quad (4.4)$$

$$c = \text{erf} \left(\frac{Pe}{2} \right) \frac{1}{r} \sin \frac{\theta}{2} \quad (4.5)$$

where we have shifted the velocity potential, $\phi = f(z)^2 - 2 = z + z^{-1}$. Far from the rim, we recover the half-plate similarity solution, since $f(z) \sim z^{1/2}$ as $|z| \rightarrow \infty$, but close to the rim, as shown in Fig. 3, there is a nontrivial dependence on Pe . For $Pe \gg 1$, a boundary layer of $O(Pe^{-1/2})$ thickness forms on the front of the rim and extends to within an $O(Pe^{-1/2})$ distance from the rear stagnation point.

The flux density is easily calculated in the w -plane and then mapped to the z -plane using Eq. (2.7):

$$F_z = -2f'(z)f(z)PeS = -\frac{Pe}{f'(z)} \text{Im } f(z) - \frac{Pe}{f'(z)} S^0 = -\frac{Pe}{f'(z)} \text{Im } f(z) \quad (4.6)$$

where the first term describes advection and the second, diffusion. The lines of advective and diffusive flux, which are level curves of $\text{Im } f(z)^2$ and $\text{Re } f(z)$, respectively, are independent of Pe and $b(c)$, as required by the Equivalence Theorem. In particular, the diffusive flux lines have the same shape for any flow speed or nonlinear diffusivity as in the case of simple linear diffusion ($Pe = 0$, $b(c) = 1$, $c / \text{Im } f(z)$), even though advection and nonlinearity affect the lines of total flux.

The lines of total flux, called 'heatlines' in thermal advection-diffusion, are level curves of the 'heat function' ψ (Kimura & Bejan 1983), which we define in complex notation via $rH = i\psi$. For a linear diffusivity, we integrate Eq. (4.6) to obtain the heat function for any conformal mapping,

$$H = 2 \text{Re } f(z) - \frac{Pe}{2} (\text{Im } f(z))^2 \text{erf} \left(\sqrt{\frac{Pe}{2}} \text{Im } f(z) \right) + \frac{Pe}{2} \exp \left(-\frac{Pe}{2} (\text{Im } f(z))^2 \right); \quad (4.7)$$

which shows how the total-flux lines cross over smoothly from fluid streamlines outside the diffusion layer ($H = \frac{Pe}{2} \text{Im } f(z)^2$, $Pe \text{Im } f(z) \gg 1$) to diffusive-flux lines near the absorbing surface ($H = 2 \text{Re } f(z)$, $Pe \text{Im } f(z) \ll 1$).

On the absorbing surface, $\text{Im } f(z) = 0$, the flux density is purely diffusive and in the normal direction. Its spatial distribution is determined geometrically by the conformal map,

$$F_z = \sqrt{\frac{Pe}{2}} S^0(0) \bar{f}^0(z) \quad \text{on } \text{Im } f(z) = 0; \quad (4.8)$$

and only its magnitude depends on Pe , as predicted by the Equivalence Theorem. (For a linear diffusivity, $S^0(0) = 2\sqrt{\frac{Pe}{2}}$.) What appears to be the only previous result of this kind is due to Koplik et al. (1994, 1995) in the context of tracer dispersion by linear advection-diffusion in porous media. In the case of planar potential flow from a dipole source to an equipotential absorbing sink, they proved that the spatial distribution of surface flux is independent of Pe . Here we see that the same conclusion holds for all similarity solutions to Eq. (4.1), even if (i) diffusive flux is not directed along streamlines; (ii) the diffusivity is a nonlinear function of the concentration; and (iii) the domain is on a curved surface.

(b) Streamline Coordinates

In proving their equivalence theorem, Koplik et al. (1994, 1995) transform Eq. (4.1) in the linear case, $b(c) = 1$, to 'streamline coordinates',

$$Pec = c + c^* \quad ; \quad (4.9)$$

where $\phi = \psi + i\chi$ is the complex potential, ψ , the velocity potential, and χ , the stream function. Because the independent and dependent variables are interchanged,

Sen & Yang (2000) have recently shown that the heat function satisfies Laplace's equation, $r^2 H = 0$, in certain potential-dependent coordinates, $r = e^{Pe \chi}$. This might seem related to our theorems, but it does not provide a basis for conformal mapping of the domain because the coordinate transformation is not analytic. Its value is also limited by the fact that the boundary conditions on H are not known a priori. For example, on a surface where the concentration is specified, the unknown flux is also required. These difficulties underscore the fact that the solutions of Eq. (4.1) are fundamentally non-harmonic.

this is a type of hodographic transformation (Whitham 1974; Ben Amar & Poire 1999). The physical interpretation of Eq. (4.9) is that advection (the left-hand side) is directed along stream lines, while diffusion (the right-hand side) is also perpendicular to the stream lines, along iso-potential lines. In high-Reynolds-number fluid mechanics, this is a well known trick due to Boussinesq (1905) still in use today (Hunt & Eames 2002). Stream line coordinates are also used in Maksimov's method for dendritic solidification from a flowing melt (Cummings et al. 1999).

Boussinesq's transformation is simply a conformal mapping to a geometry of uniform flow. Any obstacles in the flow are mapped to line segments (branch cuts of the inverse map) parallel to the stream lines. Among the solutions (4.3), stream line coordinates correspond to the map, $f(z) = \sqrt{z}$, from a plane of uniform flow past an absorbing flat plate on the positive real axis (the branch cut), as shown in the top right panel of Fig. 2. In this geometry, we have the boundary-value problem, $Pe \frac{\partial c}{\partial x} = r^2 c$, $c(x > 0; 0) = 0$, $c(-1; y) = 1$, which Carrier et al. (1983) have solved using the Wiener-Hopf technique. More simply, Greenspan has introduced parabolic coordinates (as in Greenspan 1961), to immediately obtain the similarity solution derived above, $c(x; y) = \text{erf}(\sqrt{Pe})$, where $2^2 = x + x^2 + y^2$. The reason why this solution exists, however, only becomes clear after conformal mapping to non-stream line coordinates in the upper half plane. (See also Cummings et al. 1999.)

As this example illustrates, stream line coordinates are not always convenient, so it is useful to exploit the possibility of conformal mapping to other geometries. For similarity solutions, it is easier to work in a plane where the diffusive flux lines are parallel. Stream line coordinates are also often poorly suited for numerical methods because stagnation points are associated with branch-point singularities. This is especially problematic for free boundary problems: For flows toward finite dendrites, it is easier to determine the evolving map from a half plane (Cummings et al. 1999); for flows past finite growing objects, it is easier to map from the exterior of the unit circle (Bazant, Choi & Davidovitch 2003).

(c) Non-similarity Solutions for Finite Absorbing Objects

It is tempting to try to eliminate the plate from the cylindrical rim in Fig. 3 by conformal mapping from the exterior of a finite object to the upper half plane. Any such mapping in Eq. (4.3), however, requires a quadrupole point source of flow (mapped to 1) on the object's surface. This is illustrated in the lower right panel of Fig. 2 by a Möbius transformation from the exterior of the unit circle, $f(z) = (1+z)/(1-z)$, where a source at $z = 1$ ejects concentrated fluid in the +1 direction and sucks in fluid along the -1 directions. Thus we see that, due to the boundary conditions at 1, uniform flow past an absorbing cylinder (or any other finite object) is in a different class of solutions, where the diffusive flux lines depend nontrivially on Pe . In stream line coordinates, this includes the problem of uniform flow past a finite absorbing strip, which requires solving Wijnngaarden's integroequation (Cummings et al. 1999).

Here, we study only the high- Pe asymptotics of advection-diffusion layers around finite absorbing objects. Consider again the example of flow past a cylindrical rim on a flat plate (Fig. 3). Because disturbances in the concentration decay exponentially upstream beyond an $O(Pe^{-1/2})$ distance, removing the plate on the downstream side of the cylinder has no effect in the limit $Pe \rightarrow \infty$, except on the plate itself

(the branch cut), so the solution (4.4)–(4.5) is also asymptotically valid near a finite absorbing cylinder (without the plate).

More generally, if $z = h(q)$ is the conformal map from the exterior of any singly connected finite object to the exterior of the unit circle, then the non-harmonic concentration field has the asymptotic form,

$$c(q; \bar{q}) \sim \operatorname{erf} \left(\frac{1}{\sqrt{\operatorname{Pe}}} \operatorname{Im} h(q) + \frac{1}{\sqrt{\operatorname{Pe}}} \frac{1}{h(q)} \right) \quad (4.10)$$

as $\operatorname{Pe} \rightarrow \infty$ everywhere except in the wake near the pre-image of the positive real axis, a branch cut corresponding to the ‘false plate’. The convergence is not uniform, since the false plate always spoils the approximation sufficiently far downstream, for a fixed $\operatorname{Pe} \gg 1$. The validity of Eq. (4.10) near the surface of the object, however, allows us to calculate the normal flux density using Eq. (4.8),

$$\hat{n} \cdot \nabla c \sim \frac{1}{2\sqrt{\operatorname{Pe}}} \sin \frac{\theta}{2} \quad (4.11)$$

as $\operatorname{Pe} \rightarrow \infty$ for all $\theta = \arg h(q) \neq \pi$ away from the rear stagnation point, $\theta = 0$. The limiting Nusselt number, $\operatorname{Nu} \sim \frac{1}{8} \operatorname{Pe}^{1/2}$, is also easily calculated by mapping the rim (with the false plate) to the upper half plane where the normal flux density is uniform, $\frac{1}{2\sqrt{\operatorname{Pe}}}$, on a line segment of length four (from -2 to 2).

As explained in section 2(c), Equation (4.11) describes the non-harmonic probability measure for fractal growth by steady advection-diffusion in a uniform potential flow in the limit $\operatorname{Pe} \rightarrow \infty$. This model, which we might call ‘advection-diffusion-limited aggregation’ (ADLA), is perhaps the simplest generalization of the famous DLA model of Witten and Sander (1981) allowing for more than one bulk transport process. The resulting competition between advection and diffusion produces a crossover between two distinct statistical ‘phases’ of growth. As expected from renormalization-group theory (Goldenfeld 1992), the crossover connects ‘fixed points’ of the growth measure, describing self-similar dynamics. For small initial Peclet numbers, $\operatorname{Pe}(0) \ll 1$, the growth measure of ADLA is well approximated by the uniform harmonic measure of DLA and the concentration by the similarity solution, $c(q; \bar{q}) \sim \operatorname{Im} \log h(q)$, but this is an unstable fixed point. Regardless of the initial conditions, the Peclet number diverges, $\operatorname{Pe}(t) = U L(t) = D \rightarrow \infty$, as the object grows, so the concentration eventually approaches the new similarity solution in Eq. (4.10). At this advection-dominated stable fixed point, the growth measure obeys Eq. (4.11). The $\sin \theta/2$ dependence causes anisotropic fractal growth at long times favoring the direction of incoming, concentrated fluid, $\theta = \pi$, and the total growth rate (Nu) is proportional to $\sqrt{\operatorname{Pe}(t)}$. Such analytical results serve to illustrate the power of conformal mapping applied to systems of invariant equations.

5. Electrochemical Transport

(a) Simple Approximations and Conformal Mapping

Conservation laws for gradient-driven fluxes also describe ionic transport in dilute electrolytes. Because the complete set of equations and boundary conditions

(below) are nonlinear and rather complicated, the classical theory of electrochemical systems involves a hierarchy of approximations (Newman 1991). Conformal mapping has long been applied in the simplest case where the current density, J , is proportional to the gradient of a harmonic function, ϕ , the electrostatic potential (Moulton 1905; Hine 1956).

This approximation, the 'primary current distribution', describes the linear response of a homogeneous electrolyte to a small applied voltage or current, as well as more general conduction in a supporting electrolyte (a great excess of inactive ions). The assumptions of Ohm's Law, $J = -\sigma \nabla \phi$ (with a constant conductivity, σ) and no bulk charge sources or sinks, $\nabla \cdot J = 0$, are analogous to those of potential flow and incompressibility describe above. Each electrode is assumed to be an equipotential surface (see below), so the potential is simply that of a capacitor | harmonic with Dirichlet boundary conditions. Naturally, classical conformal mapping from electrostatics (Churchill & Brown 1990; Needham 1997) have been routinely applied, but it seems conformal mapping has never been applied to any more realistic models of electrochemical systems.

The 'secondary current distribution' introduces a kinetic boundary condition, $J = R(\phi)$, which equates the normal current with a potential-dependent reaction rate, e.g. given by the Butler-Volmer equation (see below). In this case, conformal mapping could be of some use. Although the boundary condition acquires a non-constant coefficient, j^0_j , from Eq. (2.7), Laplace's equation is preserved.

A more serious complication in the 'tertiary current distribution' is to allow the bulk ionic concentrations to vary in space (but not time). Ohm's law is then replaced by a nonlinear current-voltage relation. Our main insight here is that conformal mapping can still be applied in the usual way, even though the equations are nonlinear and the potential, non-harmonic.

(b) Dilute-Solution Theory

In the usual case of a dilute electrolyte, the ionic concentrations, $c_1; c_2; \dots; c_N$, and the electrostatic potential, ϕ , satisfy the Nernst-Planck equations (Newman 1991), which have the form of Eqs. (3.1) and (3.2), where the 'advection' velocities, $u_i = z_i e \tau_i \nabla \phi$, are due to migration in the electric field, $E = -\nabla \phi$. Here, $z_i e$ is the charge (positive or negative) and τ_i the mobility of the i th ionic species. The diffusivities are given by the Einstein relation, $D_i = k_B T \tau_i$, where k_B is Boltzmann's constant and T , the temperature. Scaling concentrations to a reference value, C , potential to the thermal voltage, kT/e , length to a typical electrode separation, L , and assuming that D_i , T , and τ_i are constants, the steady-state equations take the dimensionless form,

$$\nabla^2 c_i + z_i \nabla \phi \cdot \nabla c_i = 0: \quad (5.1)$$

The ionic flux densities are $F_i = -D_i \nabla c_i - z_i c_i \nabla \phi$ (scaled to $D_i C = L$).

Because dissolved ions are very effective at charge screening, significant diffuse charge can only exist in very thin (1–100 nm) interfacial double layers, where boundary conditions break the symmetry between opposite charge carriers. The bulk potential (outside the double layers) is then determined implicitly by the condition of electroneutrality (Newman 1991), $\sum_{i=1}^N z_i c_i = 0$, which is trivially conformally invariant. Therefore, the most common model of steady electrochemical

transport, Eq. (5.1), satisfies the assumptions of the Conformal Mapping Theorem for any number of ionic species ($N \geq 2$). Although the equations differ from those of advection-diffusion in a potential flow, we can still map to electric-field coordinates (the analog of stream line coordinates), or any other convenient geometry.

Although the equations are conformally invariant, the boundary conditions are so only in certain limits. General boundary conditions express mass conservation, either $\hat{n} \cdot \mathbf{F} = 0$ for an inert species, or

$$\hat{n} \cdot \mathbf{r} \cdot \mathbf{F} = R_i(c_i; \phi); \quad (5.2)$$

for an active species at an electrode, where $R_i(c_i; \phi)$ is the Faradaic reaction-rate density (scaled to $D_i C = L$). It is common to assume Arrhenius kinetics,

$$R_i(c_i; \phi) = k_+ c_i e^{z_i(\phi - \phi_e)} - k_- c_r e^{-z_i(\phi - \phi_e)} \quad (5.3)$$

where k_+ and k_- are rate constants for deposition and dissolution, respectively (scaled to $D_i L$), ϕ_e are transfer coefficients, c_r is the concentration of the reduced species (scaled to C) and ϕ_e is the electrode potential (scaled to kT/e). Taking diffuse interfacial charge into account somewhat modifies $R(c_i; \phi)$, but the basic structure of Eq. (5.2) is unchanged (Newman 1991; Bonnefont et al. 2001). Conformal mapping introduces a non-constant coefficient, ϕ^0 , in Eq. (5.2), but conformal invariance is restored in the case of 'fast reactions' ($k_+ \gg 1$; $k_- \gg 1$), in which equilibrium conditions prevail, $R = 0$, even during the passage of current. For a single active species (say $i = 1$), the bulk potential at an electrode is then given by the (dimensionless) Nernst equation,

$$\phi_e = \phi_{eq} = \frac{\log(k c_1)}{z_1(\alpha_+ + \alpha_-)}; \quad (5.4)$$

where $k = k_+ = k_-$ is an equilibrium constant.

(c) Conformal Mapping with Concentration Polarization

The voltage across an electrochemical cell is conceptually divided into three parts (Newman 1991): (i) the 'Ohmic polarization' of the primary current distribution, (ii) the 'surface polarization' of the secondary current distribution, and (iii) 'concentration polarization', the remaining voltage attributed to non-uniform bulk concentrations. Although concentration polarization can be significant, especially at large currents in binary electrolytes, it is difficult to calculate. Analytical results are available only for very simple geometries (mainly in one dimension), so our method easily produces new results.

For example, consider a symmetric binary electrolyte ($N = 2$) of charge number, $z = z_+ = -z_- = z$, where the concentration, $c = c_+ = c_-$, and the potential satisfy,

$$r^2 c = 0 \quad \text{and} \quad r \cdot (\nabla \phi) = 0; \quad (5.5)$$

(The concentrations are harmonic only for $N = 2$.) Assuming that anions are chemically inert yields an invariant zero-flux condition at each electrode, $\hat{n} \cdot (\nabla \phi)$

Expressing Eq. (5.3) in terms of the 'surface overpotential', $\phi_s = \phi_e - \phi_{eq}$, yields the more familiar Butler-Volmer equation (Newman 1991).

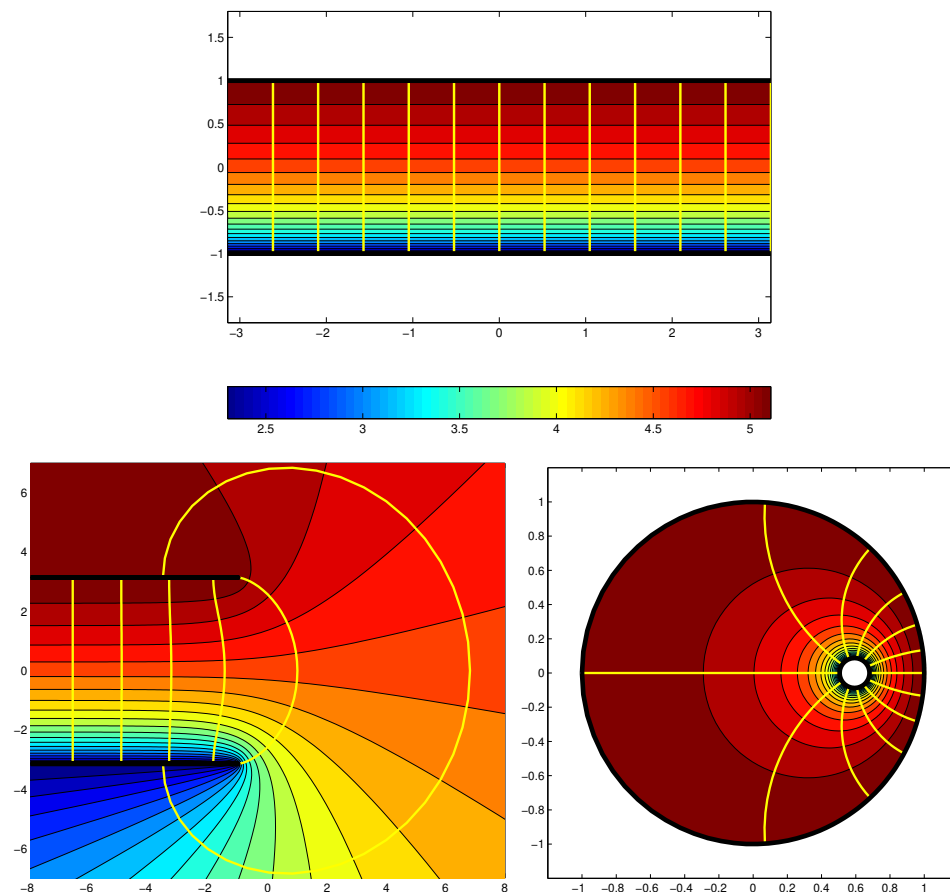


Figure 4. Similarity solutions for the electrostatic potential (contour plot) and current/electric field lines (yellow) in a binary electrolyte at 90% of the limiting current ($k = 1$). The simple solution for parallel-plate electrodes (top) is conformally mapped to semi-infinite plates (bottom left) and misaligned coaxial cylinders (bottom right).

$c = 0$, and (to break degeneracy) a constraint on the integral of c , which sets the total number of anions (Bonnefont et al. 2001). In the limit of fast reactions, the bulk potential at each electrode is given by the Nernst equation, $\phi = \phi_0 - \log kc$, where we scale ϕ to $k_B T = ze$ and assume $\phi_0 = 1$.

A class of similarity solutions is obtained by conformal mapping, $w = f(z)$, to a strip, $-1 < \text{Im } w < 1$, representing parallel-plate electrodes. We set $\phi = 0$ at the cathode ($\text{Im } w = -1$) and $\phi = V$, the applied voltage (in units of $k_B T = ze$), at the anode ($\text{Im } w = 1$). We then solve $c^{(0)} = 0$ and $(c^{(0)})' = 0$ with appropriate boundary conditions to obtain a general solution for any conformal mapping to the strip:

$$c = 1 + J \text{Im } f(z); \quad \phi = \log \frac{1 + J \text{Im } f(z)}{k(1 - J^2)}; \quad (5.6)$$

where $J = \tanh(V/4)$ is the uniform current density in the strip, scaled to its limiting value, $J_{\text{lim}} = 2zeD + C = L$. As $J \rightarrow 1$, strong concentration polarization

develops near the cathode, as shown in Fig. 4 for $J = 0.9$. At $J = 1$, the bulk concentration at the cathode vanishes, and the cell voltage diverges due to diffusion limitation.

The classical conformal map, $z = f^{-1}(w) = w + e^{-w}$ (Churchill & Brown 1990), unfolds the strip like a 'fan' to cover the z -plane and maps the electrodes onto two halfplates ($\text{Im } z = 0, \text{Re } z < 1$). As shown in Fig. 4, this solution describes the fringe fields of semi-infinite, parallel-plate electrodes. The field and current lines are cycloids, $z_a(\theta) = a + i + e^a e^{i\theta}$, as in the limit of a harmonic potential at low currents, $J \text{Im } f(z) \rightarrow \log k$. At high currents, the magnitude of the electric field is greatly amplified near the cathode (the lower plate) by concentration polarization, but the shape of the field lines is always the same. This conclusion also holds for all other conformal mappings to the strip, such as the Möbius-log transformation, $w = f(z) = i(1 + \log(5z - 3)) = (5 - 3z)i$, in Fig. 4 from the region between two non-concentric circles.

It is interesting to note that the Equivalence Theorem applies to some physical situations and not others. Similarity solutions like the ones above can only be derived for two equipotential electrodes by conformal mapping to a strip, where the current is uniform. In all such geometries, the electric field lines have the same shape as in the primary current distribution. For three or more equipotential electrodes, however, this is no longer true because conformal mapping to the strip is topologically impossible, and thus similarity solutions do not exist. When the bulk potential varies at the electrodes according to Eq. (5.2), the electric field lines generally differ from both the primary and secondary current distributions, even for just two electrodes.

6. Conclusion

We have observed that the nonlinear system of equations (2.4) involving 'dot products of two gradients' is conformally invariant. This has allowed us to extend the classical technique of conformal mapping to some non-harmonic functions arising in physics. Examples from transport theory are steady conservation laws for gradient-driven fluxes, Eq. (3.2). For one variable, the equations in our class (including some familiar examples in nonlinear diffusion) can always be reduced to Laplace's equation. For two or more variables, the general solutions are not simply related to harmonic functions, but all similarity solutions exhibit an interesting geometrical equivalence.

For two variables, there is one example in our class, steady advection-diffusion in a potential flow, to which conformal mapping has previously been applied. In this case, our method is equivalent to Boussinesq's stream line coordinates, but somewhat more general. A nonlinear diffusivity is also allowed, and the mapping need not be to a plane of uniform flow (parallel stream lines). In a series of examples, we have considered flows past absorbing leading edges and have generalized a recent equivalence theorem of Koplik, Redner, and Hinch (1994, 1995). We have also considered the flows past finite absorbing objects at high Peclet number.

Our class also contains the Nernst-Planck equations for steady, bulk electrochemical transport, for which very few exact solutions are known in more than one dimension. In electrochemistry, conformal mapping has been applied only to harmonic functions, so we have presented some new results, such as the concentration

polarizations for semi-infinite, parallel-plate electrodes and for misaligned coaxial electrodes. More generally, we have shown that Ohm's Law gives the correct spatial distribution (but not the correct magnitude) of the electric field on any pair of equipotential electrodes in two dimensions, even if the transport is nonlinear and non-Laplacian, although this is not true for three or more electrodes. Such results could be useful in modeling micro-electrochemical systems, where steady states are easily attained (due to short diffusion lengths) and quasi-planar geometries are often arise.

As mentioned throughout the paper, our results can be applied to a broad class of moving free boundary problems for systems of non-Laplacian transport equations (Bazant, Choi & Davidovitch 2003). In contrast, the vast literature on conformal mappings (cited in section 1) relies on complex-potential theory, which only applies to Laplacian transport processes. Nevertheless, standard formulations, such as the Polubarinova-Galin equation for continuous Laplacian growth (Howison 1992) and the Hastings-Levitov (1998) method of iterated maps for DLA, can be easily generalized for coupled non-Laplacian transport processes in our class. In the stochastic case, non-harmonic probability measures for fractal growth can be defined on any convenient contour, such as the unit circle. As an example, we have derived the stable fixed point of the growth measure for an arbitrary absorbing object in a uniform background potential flow, Eq. (4.11). This sets the stage for conformal mapping simulations of ADLA, which might otherwise seem intractable.

The author is grateful to J. Choi for the color figures; A. Ajdari, M. Ben Amar, J. Choi, K. Chu, D. Crowdy, B. Davidovitch, I. Eames, E. J. Hinch, H. K. Moffatt, and A. Toomre for helpful comments on the manuscript; MIT for a junior faculty leave; and ESPCI for hospitality and support through the Paris Sciences Chair. This work was also supported by the MRSEC Program of the National Science Foundation under award number DMR-02-13282.

References

- Ball, R. C. & Somfai, E. 2002 Theory of diffusion controlled growth. *Phys. Rev. Lett.* 89, art. no. 135503.
- Batchelor, G. K. 1967 *An introduction to fluid dynamics*. Cambridge: Cambridge University Press.
- Barra, F., Davidovitch, B. & Procaccia, I. 2002a Iterated conformal dynamics and Laplacian growth. *Phys. Rev. E* 65, art. no. 046144.
- Barra, F., Hentschel, H. G. E., Levermann, A. & Procaccia, I. 2002b Quasistatic fractures in brittle media and iterated conformal maps. *Phys. Rev. E* 65, art. no. 045101.
- Barenblatt, G. I. 1995 *Scaling, self-similarity, and intermediate asymptotics*. Cambridge: Cambridge University Press.
- Bazant, M. Z., Choi, J. & Davidovitch, B. 2003 Dynamics of conformal maps for a class of non-Laplacian growth phenomena, *Phys. Rev. Lett.* 91, art. no. 045503.
- Bedia, M. A. & Ben Amar, M. 1994 Investigations of the dendrite problem at zero surface tension in 2D and 3D geometries. *Nonlinearity* 7, 765{776.
- Ben Amar, M. 1991 Exact self-similar shapes in viscous fingering. *Phys. Rev. A* 43, 5724{5727.

- Ben Amar, M. & Brener, E. 1996 Laplacian and diffusional growth: A unified theoretical description for symmetrical and parity-broken patterns. *Physica D* 98, 128{138.
- Ben Amar, M. & Poire, E. C. 1999 Pushing a non-Newtonian fluid in a Hele-Shaw cell: From fingers to needles. *Phys. Fluids* 11, 1757{1767.
- Bensimon, D., Kadano, L. P., Shraiman, B. I. & Tang, C. 1986 Viscous flows in two dimensions *Rev. Mod. Phys.* 58, 977{999.
- Bonnefont, A., Argoul, F., & Bazant, M. Z. 2001 Asymptotic analysis of diffusion-layer effects on time-dependent interfacial kinetics. *J. Electroanal. Chem.* 500, 52{61.
- Boussinesq, M. J. 1905 Sur le pouvoir refroidissant d'un courant liquide ou gazeux. *J. de Math.* 1, 285{290.
- Burgers, J. M. 1948 A mathematical model illustrating the theory of turbulence. *Adv. Appl. Mech.* 1, 171{199.
- Carrier, G., Krook, M., & Pearson, C. E. 1983 *Functions of a complex variable*. Ithaca, New York: Hod Books.
- Chan, R. H., Delillo, T. K. & Horn, M. A. 1997 Numerical solution of the biharmonic equation by conformal mapping. *SIAM J. Sci. Comp.* 18, 1571{1582.
- Churchill, R. V. & Brown, J. W. 1990 *Complex variables and applications*, 5th edn. New York: McGraw-Hill.
- Crank, J. 1975 *Mathematics of diffusion*, 2nd edn. Oxford: Clarendon Press.
- Crowdy, D. 1999 A note on viscous sintering and quadrature identities. *Eur. J. Appl. Math.* 10, 623{634.
- Crowdy, D. 2002 Exact solutions for the viscous sintering of multiply connected fluid domains. *J. Eng. Math.* 42, 225{242.
- Cummings, L. M., Hohlov, Y. E., Howison, S. D. & Komev, K. 1999 Two-dimensional solidification and melting in potential flows. *J. Fluid Mech.* 378, 1{18.
- Dai, W.-S., Kadano, L. P. & Zhou, S.-M. 1991 Interface dynamics and the motion of complex singularities. *Phys. Rev. A* 43, 6672-6682.
- Davidovitch, B., Hentschel, H. G. E., Olami, Z., Procaccia, I., Sander, L. M. & Somfai, E. 1999 DLA and iterated conformal maps. *Phys. Rev. E* 59, 1368{1378.
- Davidovitch, B., Feigenbaum, M. J., Hentschel, H. G. E. & Procaccia, I. 2000 Conformal dynamics of fractal growth patterns without randomness. *Phys. Rev. E* 62, 1706{1715.
- Eames, I. & Bush, J. W. M. 1999 Long dispersion by bodies fixed in a potential flow. *Proc. Roy. Soc. A* 455, 3665{3686.
- Entov, V. M. & Etingof, P. I. 1991 Bubble contraction in Hele-Shaw cells. *Quart. J. Mech. Appl. Math.* 44, 507{535.
- Entov, V. M. & Etingof, P. I. 1997 Viscous flows with time-dependent free boundaries in a non-planar Hele-Shaw cell. *Euro. J. Appl. Math.* 8, 23{35.
- Feigenbaum, M. J., Procaccia, I. & Davidovitch, B. 2001 Dynamics of finger formation in Laplacian growth without surface tension. *J. Stat. Phys.* 103, 973{1007.
- Galin, L. A. 1945 Unsteady filtration with a free surface. *Dokl. Akad. Nauk. S.S.S.R.* 47, 2446{249 (in Russian).
- Goldenfeld, N. 1992 *Lectures on Phase Transitions and the Renormalization Group*. Reading, Massachusetts: Perseus Books.
- Greenspan, H. P. 1961 On the flow of a viscous electrically conducting fluid. *Quart. J. Appl. Math.* 18, 408{411.
- Hastings, M. & Levitov, L. S. 1998 Laplacian growth as one-dimensional turbulence. *Physica D* 116, 244{252.
- Hastings, M. B. 2001 Fractal to nonfractal phase transition in the Dielectric Breakdown Model. *Phys. Rev. Lett.* 87, art. no. 175502.

- Hine, F., Yoshizawa, S. & Okada, S. 1956 Effects of walls of electrolytic cells on current distribution. *J. Electrochem. Soc.* 103, 186{193.
- Howison, S.D. 1986 Fingering in Hele-Shaw cells. *J. Fluid Mech.* 167, 439{453.
- Howison, S.D. 1992 Complex variable methods in Hele-Shaw moving boundary problems. *Euro. J. Appl. Math.* 3, 209{224.
- Hunt, J.C.R. & Eames, I. 2002 The disappearance of laminar and turbulent wakes in complex flows. *J. Fluid Mech.* 457, 111{132.
- Ivantsov, G.P. 1947 *Dokl. Akad. Nauk. S.S.S.R.* 58, 567 (in Russian).
- Kardar, M., Parisi, G. & Zhang, Y.-C. 1986 Dynamic scaling of growing interfaces. *Phys. Rev. Lett.* 56, 889{892.
- Kessler, D.A., Koplik, J. & Levine, H. 1988 Pattern selection in fingered growth phenomena. *Adv. Phys.* 37, 255{339.
- Kinura, S. & Bejan, A. 1983 The 'heatline' visualization of convective heat transfer. *AMSE J. Heat Transfer* 105, 916{919.
- Koplik, J., Redner, S. & Hinch, E.J. 1994 Tracer dispersion in planar multipole flows. *Phys. Rev. E* 50, 4650{4667.
- Koplik, J., Redner, S. & Hinch, E.J. 1995 Universal and nonuniversal first-passage properties of planar multipole flows. *Phys. Rev. Lett.* 74, 82{85.
- Kornev, K. & Mukhamadullina, G. 1994 Mathematical theory of freezing for flow in porous media. *Proc. Roy. Soc. London A* 447, 281{297.
- Moulton, H.F. 1905 Current flow in rectangular conductors. *Proc. London Math. Soc.* (ser. 2) 3, 104{110.
- Morega, M. & Bejan, A. 1994 Heatline visualization of forced convection in porous media. *Int. J. Heat Fluid Flow* 36, 42{47.
- Morse, P.M. & Feshbach, H. 1953 *Methods of theoretical physics*. New York: McGraw-Hill.
- Muskhelishvili, N.I. 1953 *Some basic problems in the mathematical theory of elasticity*. Groningen, Netherlands: Noordhoff.
- Needham, T. 1997 *Visual complex analysis*. Oxford: Clarendon Press.
- Newman, J. 1991 *Electrochemical systems*, 2nd. edn. Englewood Cliffs, NJ: Prentice-Hall.
- Niemeyer, L., Pietronero, L. & Wiesmann, H.J. 1984 *Phys. Rev. Lett.* 52, 1033{1036.
- Polubarinova-Kochina, P.Ya. 1945a *Dokl. Akad. Nauk. S.S.S.R.* 47, 254{257 (in Russian).
- Polubarinova-Kochina, P.Ya. 1945b *Prikl. Matem. Mech.* 9, 79{90 (in Russian).
- Saman, P.G. 1986 Viscous fingering in Hele-Shaw cells. *J. Fluid Mech.* 173, 73{94.
- Saman, P.G. & Taylor, G.I. 1958 The penetration of a fluid into a porous medium or Hele-Shaw cell containing a more viscous liquid. *Proc. R. Soc. London A* 245, 312{329.
- Sen, M. & Yang, K.T. 2000 Laplace's equation for convective scalar transport in potential flow. *Proc. Roy. Soc. Lond. A* 456, 3041{3045.
- Shraiman, B.I. & Bensimon, D. 1984 Singularities in nonlocal interface dynamics. *Phys. Rev. A* 30, 2840{2842.
- Somfai, E., Sander, L.M. & Ball, R.C. 1999 Scaling and crossovers in diffusion aggregation. *Phys. Rev. Lett.* 83, 5523{5526.
- Stepanov, M.G. & Levitov, L.S. 2001 Laplacian growth with separately controlled noise and anisotropy. *Phys. Rev. E* 63, art. no. 061102.
- Tanveer, S. 1987 Analytical theory for the selection of a symmetrical Saffman-Taylor finger in a Hele-Shaw cell. *Phys. Fluids* 30, 1589{1605.
- Tanveer, S. 1993 Evolution of Hele-Shaw interface for small surface tension. *Phil. Trans. R. Soc. London A* 343, 155{204.
- Trefethen, L.N. 1986 *Numerical conformal mapping*. Amsterdam: North Holland.
- Whitham, G.B. 1974 *Linear and nonlinear waves*. New York: Wiley.
- Witten, T.A. & Sander, L.M. 1981 Diffusion-limited aggregation: A kinetic critical phenomenon. *Phys. Rev. Lett.* 47, 1400{1403.